

Contents lists available at [ScienceDirect](https://www.sciencedirect.com)

Quaternary International

journal homepage: www.elsevier.com/locate/quaint

Modeling of Indian monsoon extremes during 850-2000AD using the proxy-data from speleothems

Pramod Kumar^a, Ashok Priyadarshan Dimri^{a,*}, Sampat Kumar Tandon^b

^a School of Environmental Sciences, Jawaharlal Nehru University, New Delhi, India

^b Earth and Environmental Sciences, Indian Institute of Science Education and Research, Bhopal, India

ARTICLE INFO

Keywords:

Speleothems
Droughts
Surface energetics
Radiative flux
Sensible heat
Latent heat

ABSTRACT

This work highlights the potential significance of palaeoclimate model outputs in explaining the physical processes and mechanisms to better understand the speleothem-based proxy records of the precipitation and temperature signals during the Indian northeast and southwest monsoon from 850 to 2000AD. Thus, discussion is mainly focused on this conception by providing insights for aligning modeling preferences with the proxy records. $\delta^{18}\text{O}$ speleothem values show that precipitation over northeast India (NEI) remained constantly higher than that over the summer core monsoon zone (CMZ) from 850-2000AD. Based on the dynamical numerical coupled model (CSIRO-Mk3L-1-2) outputs, the data are in alignment with the presence of four proxy-based major extreme climatic events: Dry Century (DC), Medieval Climatic Anomaly (MCA), Extreme Dry Century (EDC) and Little Ice Age (LIA) during the last millennia. In these extremes a significant trend in diurnal temperature range (DTR), in particular, is correspondingly observed. These extremes and associated mechanisms are examined using surface energetics and corresponding atmospheric-oceanic coupled processes. The analysis of downward radiative (shortwave and longwave), latent and sensible heat fluxes provided better rationale and understanding of associated physical processes and mechanisms. It is found that the latent and sensible heat fluxes were balanced by downward radiative fluxes and the remaining part of energy was anomalously trapped inside the surface, thus reflecting anomalous climatic behavior during these extremes.

1. Introduction

Long term precipitation and temperature variations spanning the last ~2000 years have been studied based on speleothem records (Jones et al., 1998; Briffa, 2000; Crowley and Lowery, 2000; Esper et al., 2002; Cook et al., 2003; Mann and Jones, 2003; Mann et al., 2008; 2009; Jones and Mann, 2004; Moberg et al., 2005; D'Arrigo et al., 2006; Osborn and Briffa, 2006; Loehle, 2007; Hegerl et al., 2007; Juckes et al., 2007; Sinha et al., 2007; Ljungqvist, 2010; Dixit and Tandon, 2016; Kathayat et al., 2016, 2019; Kumar et al., 2019). This period contains two significant climatic change episodes: the warm period (Medieval Climatic Anomaly, MCA: ~900-1300AD) and the relatively cold period (LIA: ~1500-1850AD). However, MCA and LIA seem to be restricted to the circum-North Atlantic region (Hughes and Diaz, 1994a,b; Mann and Jones, 2003; Mann et al., 1999) and did not appear synchronously in other regions (Grove, 1988) as seen from the substantial variation in the inception and duration of these episodes in different parts of the globe (Bradley and Jones, 1992, 1993). The intensity of the monsoon is

generally considered to have weakened during the LIA (Anderson et al., 2002; Gupta et al., 2003), but there are evidences of wetter conditions during the LIA in the Indian Himalaya (Rühland et al., 2006; Kotlia et al., 2012, 2016), Nepal and the sites falling within similar latitudes.

The combination of palaeoclimate model outputs together with proxy-based data of speleothems provides a better and extended understanding of the climatic controls during these episodes viz., temperature, moisture and its source, precipitation amount, surface runoff, soil moisture and surface warming (Lechleitner et al., 2017). The decreased evaporation and warmer air reduces relative humidity, causing reduction in precipitation, and thus leading to low deposition of carbonates in speleothems. Reduced precipitation along with warmer land surface instigates various drought conditions (Lu et al., 2011) and can decrease soil moisture and surface runoff. Decreased precipitation lowers the infiltration processes thus creating lesser leaching of calcareous cave deposits. Therefore, the $\delta^{18}\text{O}$ concentration in the speleothems is increased, compared to $\delta^{16}\text{O}$ during lower precipitation (Gat and Gonfiantini, 1981), making this proxy unique for the reconstruction

* Corresponding author. School of Environmental Sciences, Jawaharlal Nehru University, New Delhi, 110067, India.

E-mail address: apdimri@hotmail.com (A.P. Dimri).

<https://doi.org/10.1016/j.quaint.2021.02.009>

Received 11 May 2020; Received in revised form 23 August 2020; Accepted 4 February 2021

Available online 11 February 2021

1040-6182/© 2021 Elsevier Ltd and INQUA. All rights reserved.

of the monsoon precipitation (Briffa and Jones, 1993; Sinha et al., 2007; Tejavath et al., 2017). Thus, it is important to recognize that through the application of existing palaeoclimate models and proxy-based data from speleothems, explanation of the associated physical processes and mechanisms with some degree of uncertainty can be explored.

El Niño/La Niña has also influenced monsoon during the last millennium (Wang et al., 2015; Tejavath et al., 2017, 2018). During this period, precipitation in the MCA and El Niño were negatively correlated, but were positively correlated during the LIA (Tejavath et al., 2017, 2018). The MCA was warmer and humid, whereas the LIA was colder and drier than the historical (1850-2000AD) mean climate (Yadava and

Ramesh, 2005; Tiwari et al., 2006; Veena et al., 2014; Tejavath et al., 2017). During the last millennium, the MCA and LIA are commonly accepted major extremes whereas, DC (850-950AD) and EDC (1280-1470AD) extremes are still debated. In addition, the Indian Ocean and Arabian Sea Surface Temperatures (SSTs) also play a key role in determining the strength of the monsoon (Wang et al., 2015; Ning et al., 2018). Decreasing SST drives strong winters and weak summers (Shi et al., 2008) (lesser the SST, lesser will be the evaporation leading to lesser latent heat availability in the vicinity). Warming of surface and ocean-atmosphere through anthropogenic as well as solar radiation changes have diverse signatures (Liu et al., 2013; Ning et al., 2018). The

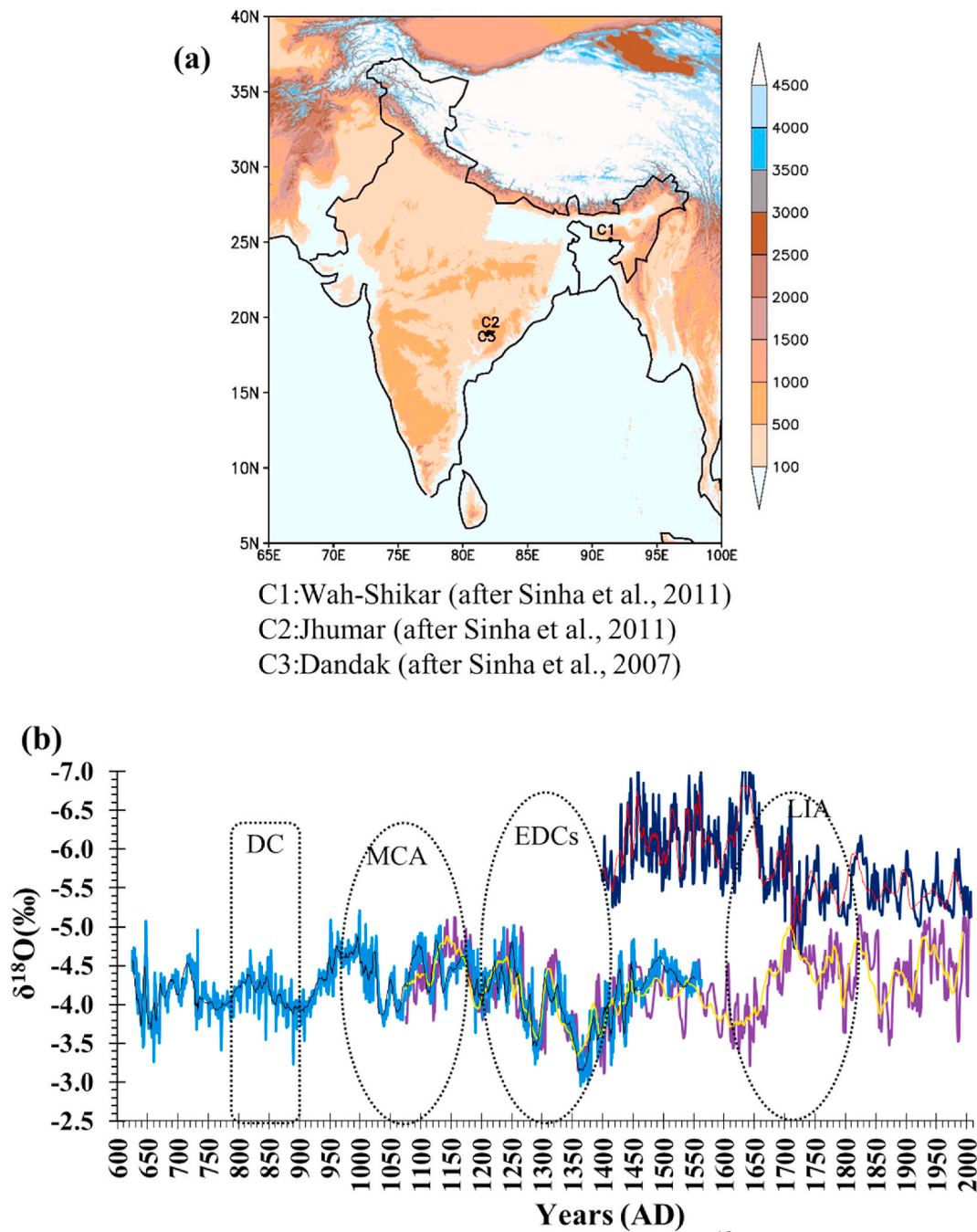


Fig. 1. (a) The cave locations and (b) corresponding speleothem $\delta^{18}\text{O}$ values for precipitation estimation from 650-2000AD period. Dry Centuries (DC: 850-951AD); Medieval Climatic Anomaly (MCA: 1050-1250AD); Extreme Dry Centuries (EDC: 1280-1470AD) and Little Ice Age (LIA: 1650-1850AD). (These extremes are marked with dashed circle). The lines correspond for Dandak: sky blue; Jhumar: purple; Wah-Shikher: dark blue. Thin lines correspond to 11 years moving average for Dandak: blue; Jhumar: yellow; Wah-Shikher: red. (Data source: Sinha et al., 2007; Berkelhammer et al., 2010). (For interpretation of the references to colour in this figure legend, the reader is referred to the Web version of this article.)

energy budget is a key control of latent heat release in precipitation and radiative heat transfer (e.g. diabatic and adiabatic heating) (Liu et al., 2013). Thus, palaeoclimate dynamics and surface energetics of above extremes during last millennium needs investigation. Only a few studies have combined observations as well as model results (e.g., Tejavath et al., 2017, 2018; Hessler et al., 2018; Li et al., 2018). Considering this, the present study aims at providing a suitable explanation of existing physical processes and coupling mechanisms for extremes viz., DC, MCA, EDC and LIA during the last millennium from 850 to 2000AD.

In the following, a brief account of the model details and proxy-based data is provided in section 2, followed by results and discussion in section 3. Finally, salient findings of the study are provided in section 4 under conclusions.

2. Brief model details and data

Proxy data from cave deposits (stalagmites) occurring in north-eastern and central India are used in the present study. The cave deposits from Wah-Shikar (in northeastern India, hereafter referred as C1), Jhumar and Dandak cave stalagmites (in central India representing CMZ, hereafter referred as C2 and C3) (Berkelhammer et al., 2010; Sinha et al., 2007, 2011) are considered (Fig. 1a). The Dandak cave speleothems represent an archive of the CMZ precipitation (Kumar et al., 2019), and that of severe droughts during 1400-1500AD (Sinha et al., 2007). The monsoon 'break' from 1400-1700AD and 'active' from 1700-2000AD have been interpreted from the proxy data of Jhumar and Wah-Shikar Cave stalagmites (Sinha et al., 2011). The $\delta^{18}\text{O}$ values of these three speleothem records are obtained from the National Oceanic and Atmospheric Administration/National Climatic Data Center (NOAA/NCDC) (Table 1). The topographic elevations and cave locations are obtained from the United States Geological Survey (USGS-GTOPO).

The CSIRO-Mk3L climate system model v1.2 (Phipps et al., 2012; hereafter referred as CSIRO-Mk3L) outputs viz., precipitation anomaly, standardized precipitation index, aridity dryness index, near surface temperature anomaly, longwave fluxes, relative humidity anomaly, diurnal temperature range and winds are considered to understand physical and dynamical processes during DC, MCA, EDC and LIA. This model has been chosen because it has better horizontal model resolution relative to other available palaeoclimate models. In addition, it is a coupled general circulation model at millennial-scale palaeoclimate simulation that includes atmosphere, land surface, ocean and sea-ice components, and offers computational efficiency with a stable and realizing control climatology. Model details and outputs are freely available (please refer to Phipps et al., 2012). Tejavath et al. (2017, 2018) discussed several GCM models including CSIRO-Mk3L, and showed that most of the models have a similar performance, but very high variability due to different model horizontal and vertical resolutions. However, this aspect is not discussed here as it is beyond the scope

Table 1
Brief of model details and data-sets used for the study.

Variables	Time period	Resolution		Source	Reference
		Temporal	Spatial		
$\delta^{18}\text{O}\text{‰}$ (VPDB) (Proxy)	850-2000 AD	± 50 years monthly	Point	NCDC	Sinha et al., 2007; Berkelhammer et al. (2010)
Latent and Sensible heat SNSR, SNTR and 2m-temperature, relative and specific humidity (CSIRO-Mk3L-1-2) moel			Point	NCDC	Berkelhammer et al. (2012)
			~200 Km	Esgf: PMIP3	Abram et al. (2014); McGregor et al. (2015); Brown et al. (2016); Phipps et al. (2012); Le (2015)

of the present paper. This model is simulated under Paleoclimate Modelling Intercomparison Project Phase III (PMIP3) for millennial timescale palaeoclimate research (Abram et al., 2014; McGregor et al., 2015; Brown et al., 2016).

3. Results and discussion

Firstly, a brief account of the cave deposits is presented, followed by the interpretation and discussion on physical processes and mechanisms associated with various palaeoclimatic events through model outputs.

Fig. 1b shows precipitation reconstruction based on speleothem carbonate $\delta^{18}\text{O}$ values from 600 to 2000AD having variable temporal extent. Based on $\delta^{18}\text{O}$ values, an approximate increase or decrease by 1.5‰ VPDB suggests dry or wet conditions (i.e., warm or cold conditions) (Yadava Madhusudan, 2002; Sinha et al., 2007). The $\delta^{18}\text{O}$ value from cave C1 (Wah-Shikar) ranges from -5.0‰ to -7.0‰ VPDB that delineates current precipitation scenario (i.e., -5.5‰ to -6.5‰ VPDB) over northeastern India (Sanwal et al., 2013). Similarly, from 650 to 2000AD $\delta^{18}\text{O}$ values ranging from -3.0‰ to -5.5‰ VPDB corresponds to caves C2 (Jhumar) and C3 (Dandak) (Sinha et al., 2007). On the basis of fluctuations of 1.5‰ VPDB in $\delta^{18}\text{O}$ values, four major events are recognized between 850 and 2000AD viz., DC, MCA, EDC and LIA (Yadava Madhusudan, 2002; Yadava and Ramesh, 2005; Tiwari et al., 2006; Sanwal et al., 2013; Veena et al., 2014; Tejavath et al., 2017). The $\delta^{18}\text{O}$ values of about -3.5‰ VPDB indicate weaker precipitation during the DC (Fig. 1b) and further enriched values of -3.0‰ VPDB, suggest very weak monsoon during the EDC.

The interpretations regarding various palaeoclimatic events are explained by different variables and indices using model outputs. The precipitation over NEI (cave C1) was always greater than that over the CMZ (caves C2 and C3). During the latter part of the LIA, precipitation decreased over NEI and relatively increased over CMZ (caves C2 and C3). During the EDC, the precipitation was comparatively higher than the current scenario. The model annual precipitation anomaly shows similar temporal variability as that obtained from speleothem based $\delta^{18}\text{O}$ proxies during 850 to 2000AD (Fig. 2). During the LIA, MCA and DC, similar precipitation variability is observed but a difference is recognized during the EDC, possibly due to the biases in the model fields as suggested earlier by Phipps et al. (2012) (in this paper, due to brevity, we are not discussing the model biases and related uncertainties). It shows positive annual precipitation anomaly from 1850 to 2000AD (i.e., similar to speleothem data base). In some of the years, there are out of phase precipitation anomalies with the corresponding proxy records. These deviations in individual years during extremes are not assessed in this study.

For further investigation, standardized precipitation index (SPI) is computed from the model outputs and shown in Fig. 3. It reveals drought conditions during the past two millennia to historical period (850-2000AD). The SPI shows higher negative peaks during the EDC and higher positive peaks during the MCA in particular when averaged over a decade (11 year running mean). However, the maximum deviation is observed during the LIA, suggesting frequent dry and wet spells. 11 year running average of SPI shows decreasing (increasing) SPI during EDC (LIA) apart from symmetrical variations. To obtain further insights, aridity dryness index (Id) from model fields is computed and presented in Fig. 4. A wide range of Id values corresponds to mild ($\text{Id} < 50$), moderate ($\text{Id} = 50-71$) and extreme arid ($\text{Id} > 72$) climatic conditions (Nagarajan, 2010). The variabilities are well captured during DC, MCA, EDC and LIA extremes. The temporal distribution of Id during 850-2000AD, including DC, MCA, EDC and LIA, corresponds to mild, moderate and extreme aridity ranges. However, temporal variation of Id values greater than 80 corresponding to the extreme arid climate, could be attributed to possible model biases. In 11 years running moving averages, these variabilities are distinctly captured (Fig. 4). The time averaged spatial extent of Id is shown in Fig. 5 during different extremes which in general, shows similar spatial distribution of Id during all the

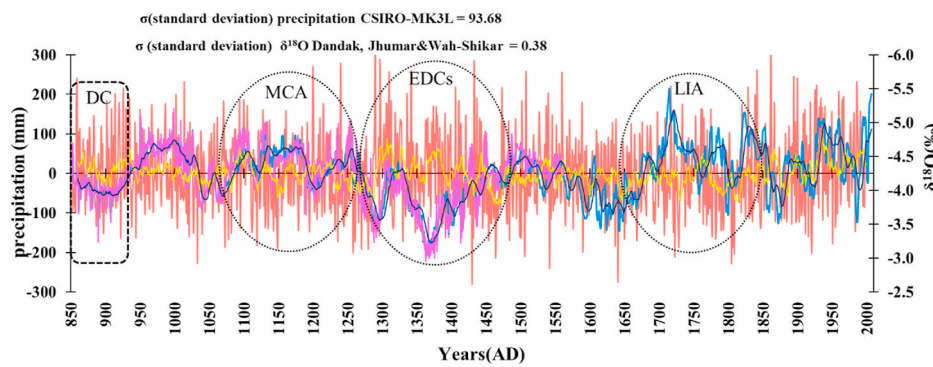


Fig. 2. Annual precipitation anomaly from model (CSIRO-MK3L: dark red line); cave deposit $\delta^{18}\text{O}$ values (from Dandak: purple line; Jhumar and Wah-Shikar: sky blue line); 11 years moving average annual precipitation anomaly from model (CSIRO-MK3L: yellow thin line) and cave deposit $\delta^{18}\text{O}$ values (from Dandak, Jhumar and Wah-Shikar: dark blue thin line) during 850-2006AD (representing DC, MCA, EDC and LIA extremes using dashed circles). All values are averaged over 65-100°E and 5-40°N. (Left side scale: precipitation anomaly (mm) and Right side scale: speleothem $\delta^{18}\text{O}$ (‰)). (Data source: [Sinha et al., 2007](#); [Berkelhammer et al., 2010](#)). (For interpretation of the references to colour in this figure legend, the reader is referred to the Web version of this article.)

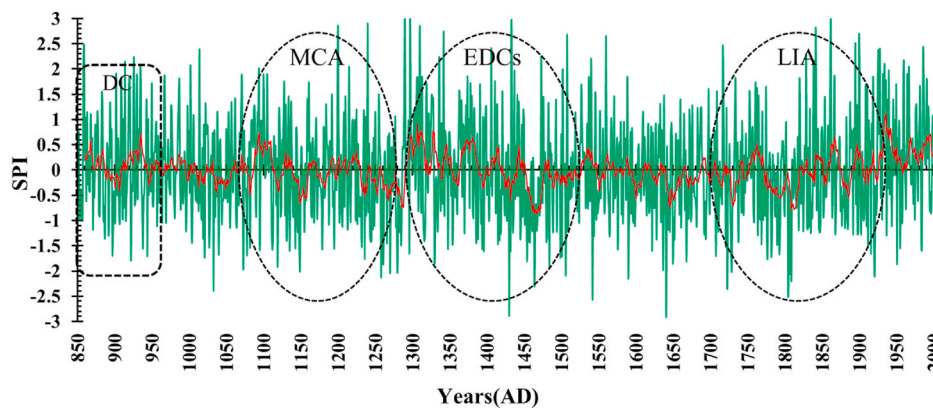


Fig. 3. Standardized precipitation index (SPI: green line); 11 years moving average of SPI (red line) using model CSIRO-MK3L during the period 850-2006AD (representing DC, MCA, EDC and LIA extremes using dashed circles). All values are averaged over 65-100°E and 5-40°N. (For interpretation of the references to colour in this figure legend, the reader is referred to the Web version of this article.)

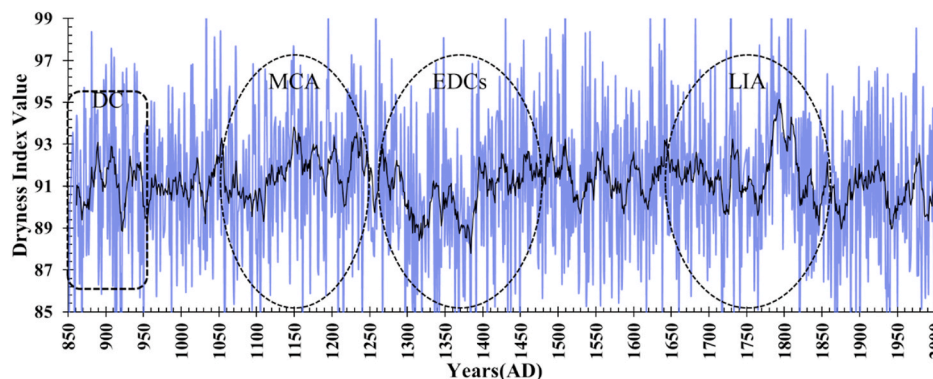


Fig. 4. Same as Fig. 3, but for aridity dryness index (Id: violet line) and 11 years moving average of Id (black line). (For interpretation of the references to colour in this figure legend, the reader is referred to the Web version of this article.)

extremes (DC: Fig. 5a, MCA: Fig. 5b, EDC: Fig. 5c and LIA: Fig. 5d). However, there are smaller differences in the spatial pattern of the Id values. In all the extremes, southwestern and eastern India shows similar pattern of lower dryness than northwestern and western India which shows relatively higher dryness. Further, these distributions are similar to that of precipitation and near surface temperature distributions, as near surface temperature is used for calculating dryness index. The near surface temperature also reveals evaporation and convection process leading to the assessment of fog/cloud forming mechanism. It depends on surface warming and cloud fraction area as well. Hence, Fig. 6 shows temporal variation of near surface temperature anomaly and cloud

fraction area during monsoon for the period 850-2000AD. It indicates higher (lower) cloud fraction area over the lower (higher) near surface temperature anomaly. This explains solar radiation trapped during the cloudy conditions when the near surface temperature is decreased anomalously; and this can be observed during all four extremes. However, near surface temperature anomalously increased during historical period (850-2000AD) but the corresponding cloud fraction area does not show much changes. Near surface temperature's anomalous increment is possibly due to pre- and post-industrial anthropogenic disturbances ([Zorita et al., 2005](#); [Liu et al., 2013](#)). The cloud forming mechanism and moisture availability along with various fluxes determine the

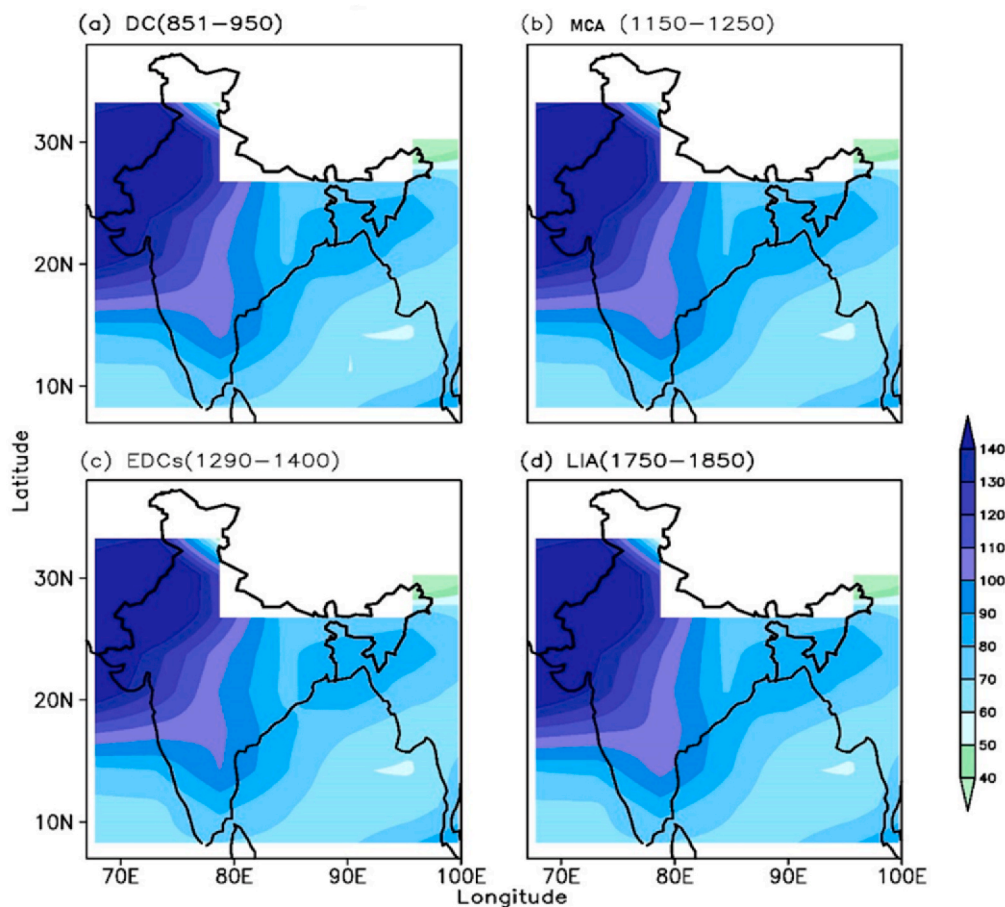


Fig. 5. Spatial extent of aridity dryness index (Id) using model CSIRO-MK3L during the period 850-2006AD representing (a) DC, (b) MCA, (c) EDC and (d) LIA extremes (White shades indicate missing data). (For interpretation of the references to colour in this figure legend, the reader is referred to the Web version of this article.)

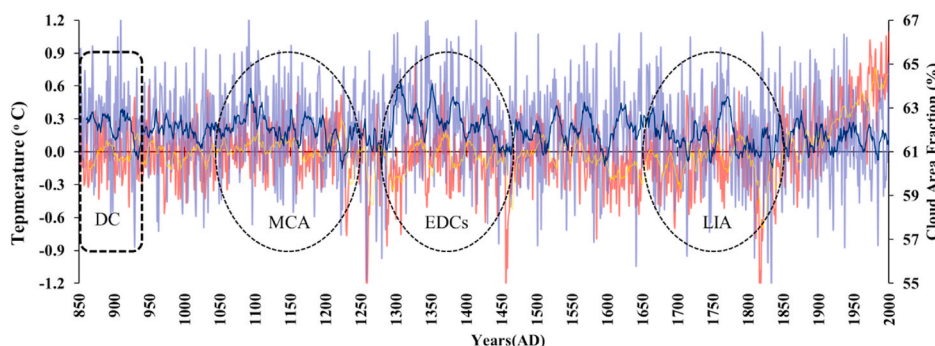


Fig. 6. Near surface temperature anomaly ($^{\circ}\text{C}$, dark red line); cloud area fraction (%), violet line); 11 years moving average of near surface temperature anomaly ($^{\circ}\text{C}$, yellow line) and cloud area fraction (%), dark blue line) using model CSIRO-MK3L during the period 850-2000AD (representing DC, MCA, EDC and LIA extremes using dashed circles). All values are averaged over 65°E and 5°N and 5°N and 40°N . (Left side scale: near surface temperature anomaly ($^{\circ}\text{C}$) and Right side scale: cloud area fraction (%)). (For interpretation of the references to colour in this figure legend, the reader is referred to the Web version of this article.)

precipitation mechanisms.

The anomalous change in cloud area fraction can cause longwave radiation upwelling trap. The increment of surface upwelling longwave flux causes a decrease in cloud area fraction. The maximum variation between cloud area fraction anomaly and surface upwelling longwave flux anomaly is observed during the EDC and LIA. However, during DC and MCA reduced variabilities between them are seen (Fig. 7). Further, cloud area fraction dependence on moisture content present in the atmosphere and air temperature feedback in terms of relative humidity distribution is analyzed. Fig. 8 shows the vertical pressure-latitude distribution of anomalous change in relative humidity (longitudinal averaged over 65°E – 100°E including ocean) during extremes (Fig. 8a–d). Reduced relative humidity in the vertical air column over 5° – 30°N is

observed during the DC; but incremental increase is observed over 31° – 40°N and beyond (Fig. 8a). However, lower level decreased relative humidity which stands increased at upper level over 20° – 40°N and beyond is observed during the MCA (Fig. 8b). An increased relative humidity distribution is seen at 800 hPa and 300 hPa over 5° – 15°N . It suggests convection over land and moisture incursion from the ocean (Fig. 8b). Decreased relative humidity distribution strongly indicates anomalous decrease in the atmospheric moisture content. A similar scenario as prevailing in the DC is observed during the EDC as well (Fig. 8c). It suggests extreme drying during monsoon i.e., a dry phase of late MCA (Sanwal et al., 2013). Fig. 8d shows decreased relative humidity over most of the regions in particular at lower levels. However, a small patch of increase is observed over 5° – 10°N at 850 hPa and 300

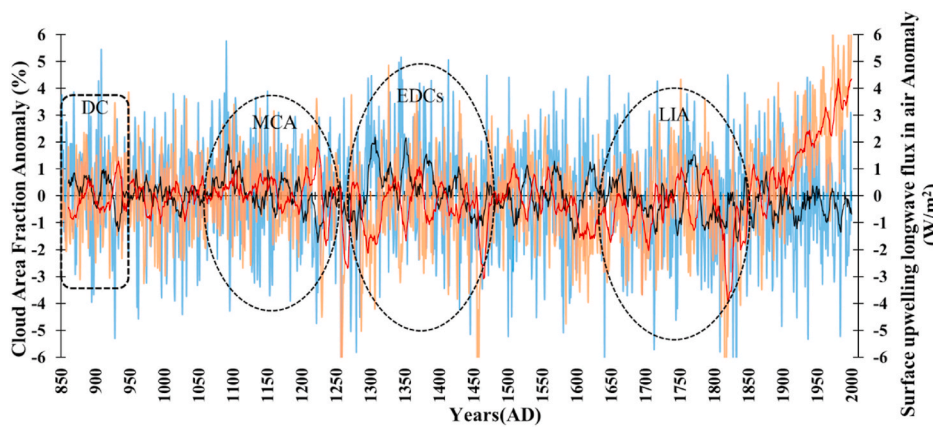


Fig. 7. Surface upwelling longwave flux in air anomaly (W/m^2 , Orange line); cloud area fraction anomaly (%), sky-blue line); 11 years moving average of surface upwelling longwave flux in air anomaly (W/m^2 , red line) and cloud area fraction anomaly (%), black line) using model CSIRO-MK3L during the period 850-2000AD (representing DC, MCA, EDC and LIA extremes using dashed circles). All values are averaged over $65\text{-}100^\circ\text{E}$ and $5\text{-}40^\circ\text{N}$. (Left side scale: cloud area fraction anomaly (%) and Right side scale: surface upwelling longwave flux anomaly (W/m^2)). (For interpretation of the references to colour in this figure legend, the reader is referred to the Web version of this article.)

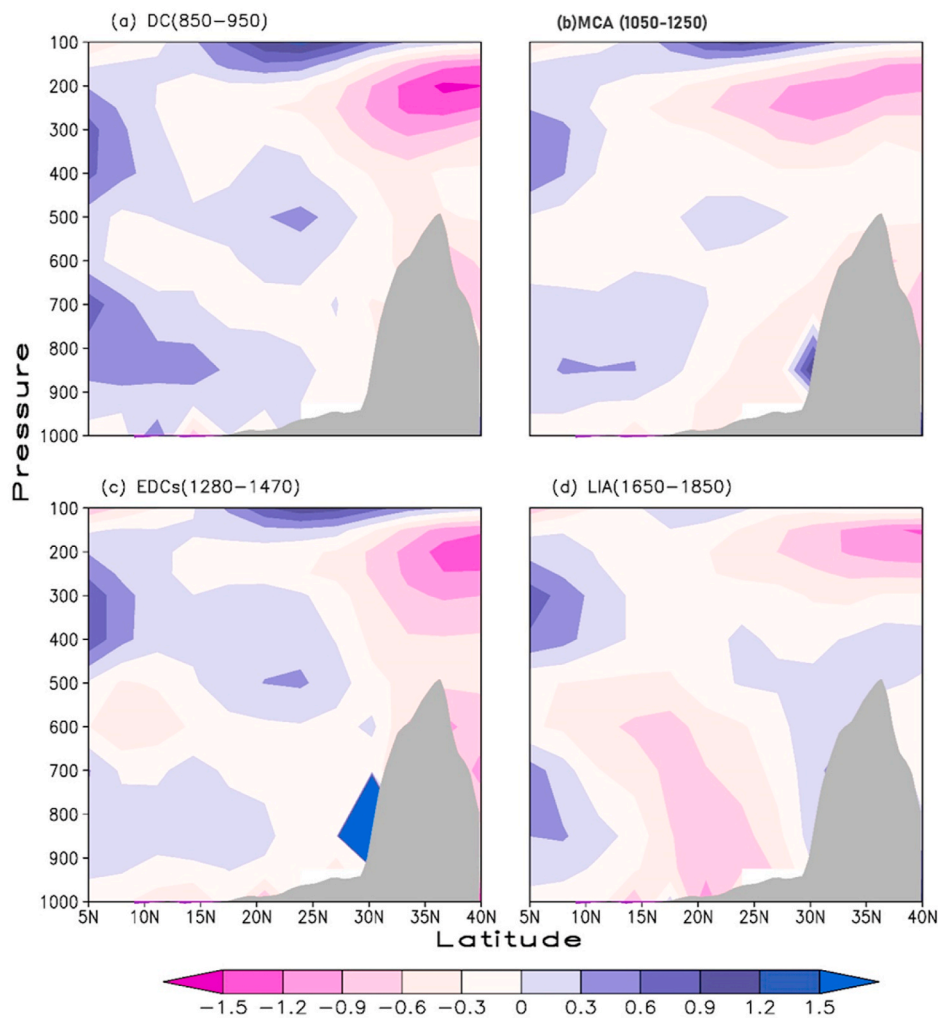


Fig. 8. Pressure – Latitude distribution of longitudinal averaged ($65^\circ\text{-}100^\circ\text{E}$) relative humidity anomaly (%) using model CSIRO-MK3L during the period 850-2000AD representing (a) DC, (b) MCA, (c) EDC and (d) LIA. Gray shade shows averaged topography of Indian subcontinent. (For interpretation of the references to colour in this figure legend, the reader is referred to the Web version of this article.)

hPa. This is possibly due to the weakening of 850 hPa Somali Jet (Rai et al., 2019) and 200 to 300 hPa Subtropical westerly Jet (Yaocun et al., 2008) (these features are not discussed here in details). In brief, weakening of Somali Jet will weaken the monsoon in tandem and similarly meridional shifting of Subtropical westerly jet too controls the amplitude of monsoon. As relative humidity is a derivative of moisture

content and temperature, diurnal temperature variation has a role in controlling it. The diurnal temperature range (DTR) shows a best distribution of warmer and colder atmosphere (Sun et al., 2017; Dimri et al., 2018). DTR distribution for the four extremes is clearly depicted in Fig. 9. During DC, strong positive trends of DTR over central India to Tibetan Plateau are observed (Fig. 9a). During MCA and EDC

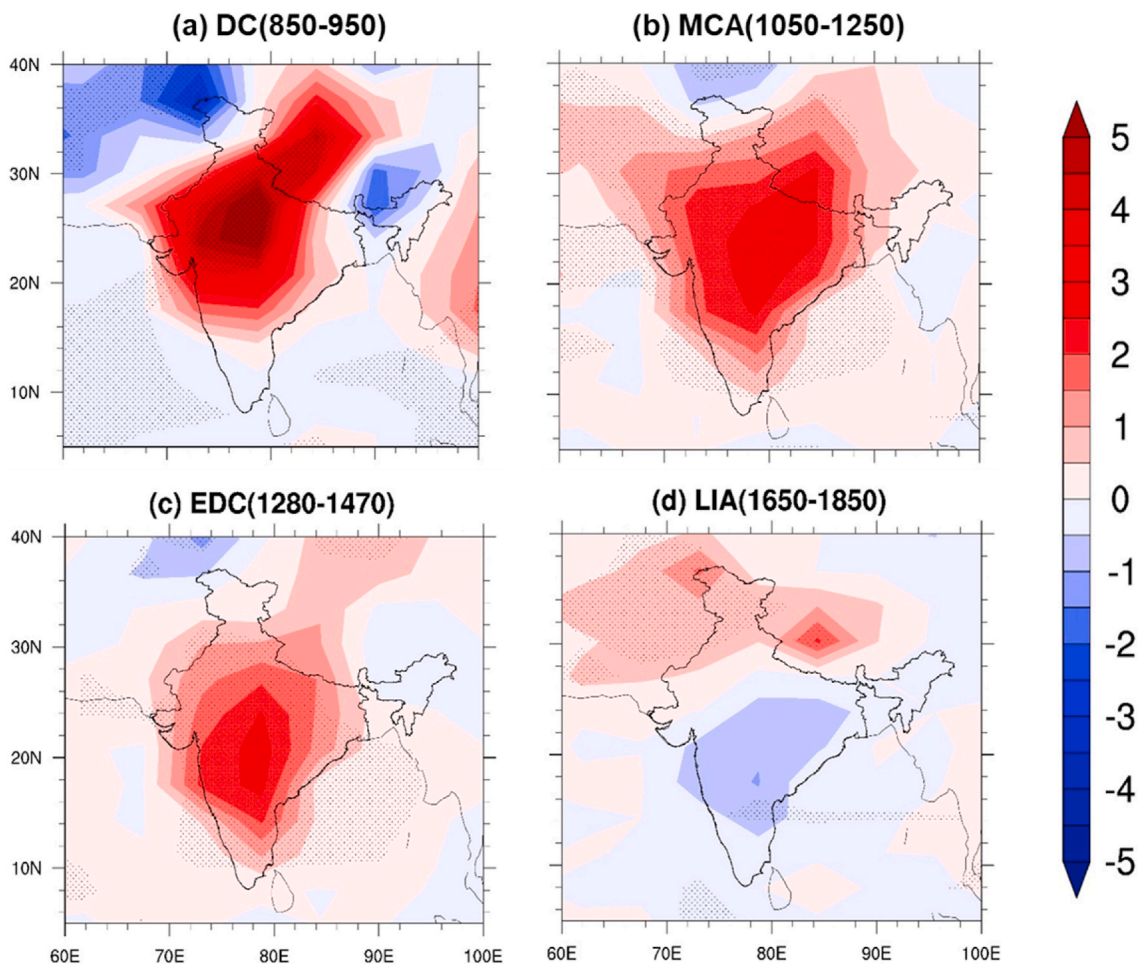


Fig. 9. Spatial extent of linear trends of diurnal temperature range (DTR, °C) using model CSIRO-MK3L during the period 850-2000AD representing (a) DC, (b) MWP, (c) EDC and (d) LIA. Trend values are complementary to 10^{-3} and patterns correspond to 75% significant.

significantly increasing trends of the DTR over the whole Indian subcontinent are observed (Fig. 9b and c), but are lower than that prevailing in the DC. However, during LIA strong negative trends all over India, south of 30°N, except over northern India (i.e., Jammu & Kashmir, Panjab and some parts of Himachal Pradesh and Rajasthan, Fig. 9d) are seen.

The corresponding temperature fields - maximum and minimum temperature - depend on a number of factors viz., cloud fraction, evapotranspiration, downwelling shortwave and downwelling longwave, amongst others (Dimri et al., 2018). The wind circulations as well play a crucial role in controlling and determining the DTR. As wind circulation during monsoon strengthens, it escalates the turbulence and mixing thus forming unstable planetary boundary layers (PBL), due to which latent and sensible heat fluxes are transferred from the surface to the atmosphere above. Fig. 10a shows 200 hPa wind climatology during DC (Fig. 10a(i)), MCA (Fig. 10a(ii)), EDC (Fig. 10a(iii)) and LIA (Fig. 10a(iv)). Almost similar 200 hPa wind patterns are seen during all extremes, except during DC, (Fig. 10a(i)). It shows different spatial extent in circulation magnitude as well as direction. In the case of lower winds, 850 hPa, during DC random circulation pattern and weaker winds are seen (Fig. 10b(i)). During MCA (Fig. 10b(ii)), and EDC (Fig. 10b(iii)), nearly similar wind circulation patterns are seen, which are strengthened during LIA, (Fig. 10b(iv)). During all these later extremes, Somali Jet got strengthened which was strongest during LIA. This was not the case during DC. Overall, during LIA similar wind directions prevail as those of MCA and EDC, with higher magnitude but with similar direction at lower level.

Further, energy is transferred from the surface to the vertical atmosphere and vice-versa. Evaporation and/or evapotranspiration processes also add on the heat transfer from surface to the atmosphere through latent heating. This makes the surface cooler after transfer of latent heat from surface to the atmosphere (Bowen, 1926; Spittlehouse and Black, 1980; Oke, 1982; Todd et al., 2000). The Arabian Sea and Bay of Bengal shows weaker latent heat flux during the monsoons in DC (Fig. S1a), indicating lesser latent heat transfer than normal from oceanic surfaces to the atmosphere (through evaporation and/or evapotranspiration). Most parts of the continental region (except Indo-Gangetic Plain) show increased or near-neutral transfer of latent heat to the atmosphere. This anomalous increased transfer of latent heat from the continental surface makes the surface drier than prevailing under normal conditions. However, during MCA, distributions are different than that of DC (Fig. S1b). Here, comparatively warmer continent and colder oceanic surfaces explain the stronger monsoon than during the DC. The EDC shows nearly similar results as during the DC (Fig. S1c). The Indian subcontinent is much warmer, suggesting extreme drier conditions during the monsoons in EDC. However, as seen in Fig. S1d, the LIA shows completely opposite distribution than that prevailing during the other three extremes (DC, MCA and EDC). As such, the whole continent shows reduced fluxes and the ocean region shows increased fluxes of latent heat. This suggests colder continent (cold and dry during LIA) relatively to warmer ocean.

Another important component, surface sensible heat flux is one of the primary drivers by which the surface energy fluxes are exchanged with the adjacent atmosphere and vice versa (Sellers, 1965; Cayan,

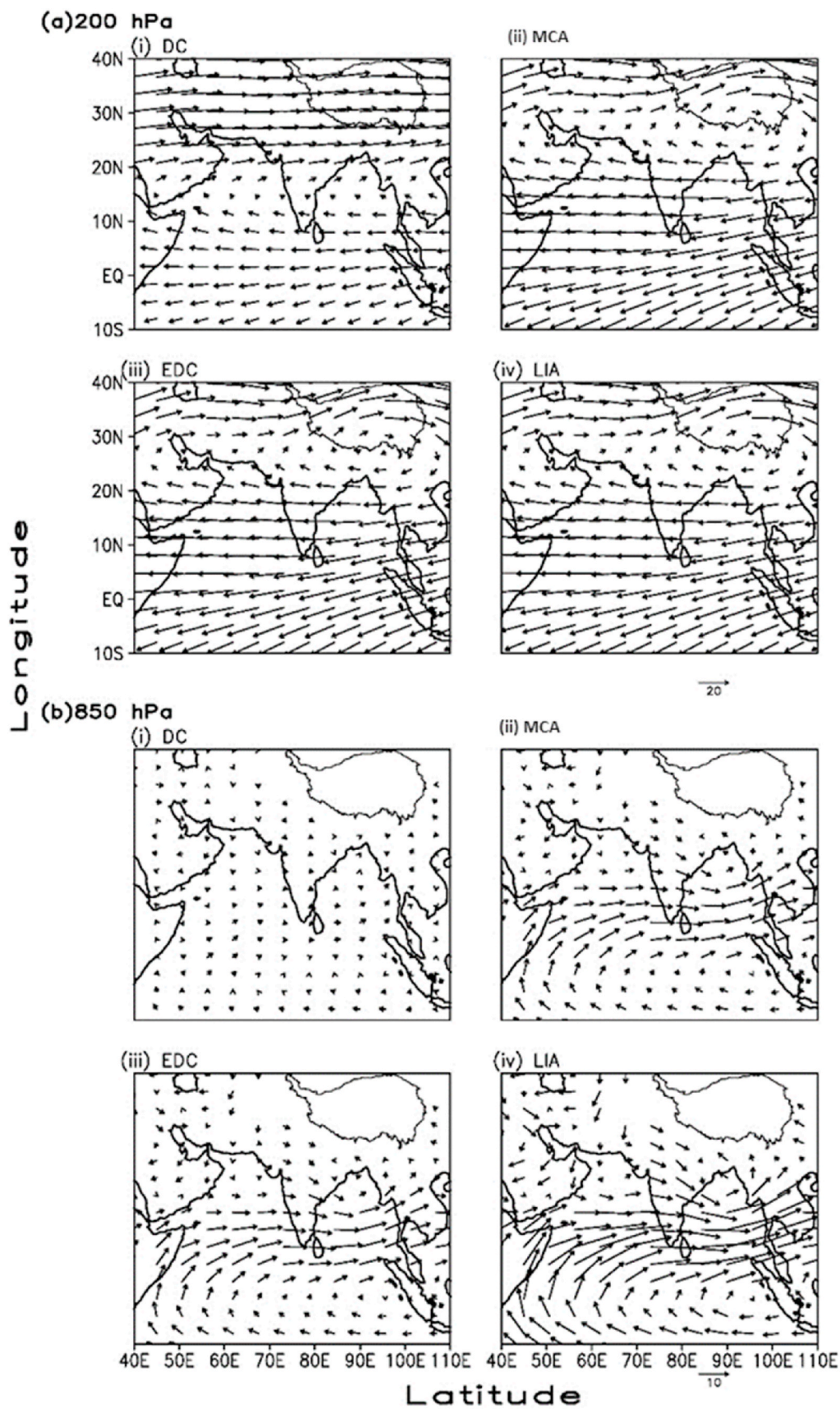


Fig. 10. Climatology of wind circulation for extremes at (a) 200 hPa during (i) DC, (ii) MCA, (iii) EDC and (iv) LIA using model CSIRO-MK3L during the period 850-2000AD. And (b) is same as (a), but for 850 hPa. (Wind speed in (a) is 20 m/s and in (b) 10 m/s respectively).

1992). The energy exchange from the surface to the atmosphere makes the atmosphere warmer through increased sensible heating (Su, 2002). During DC, reduced surface sensible heat flux over the Arabian Sea and southern India (including western Ghats and Gujarat), along with a slight increase over the Bay of Bengal (Fig. S2a) is seen. It indicates a colder Arabian Sea, with lower sensible heat transfer from the atmosphere to the surface over Western Ghats, and warmer Bay of Bengal. But the rest of the continental regions, beyond central India appear to have an increased sensible heat flux. It explains drying and heating conditions over the continent. Fig. S2b shows stronger fluxes over central India and beyond but weaker over Western Ghats during MCA. This suggests a substantial amount of energy transfer from the continent to the surrounding atmosphere during MCA. It indicates stronger evaporation and/or evapotranspiration or convection processes leading to stronger monsoon. Fig. S2c shows nearly similar exchanges but stronger sensible heat fluxes over Western Ghats, anomalous colder surface while heat is transferred from the atmosphere to the surface during the EDC, which is conducive for weaker monsoon leading to extreme dry condition. Fig. S2d shows increased fluxes over the whole region during the LIA, delineating colder surface than the atmosphere in the vicinity, and heat is transferred from the atmosphere to the surface to balance the energetics. The latent and sensible heat is released from the surface of the earth (ocean) which is absorbed from solar radiation (downward radiative flux = downwelling longwave + downwelling shortwave) (Liu et al., 2013). Figs. S3–S4 show downward radiative flux as anomalous surface downwelling shortwave flux and anomalous surface downwelling longwave flux respectively, -which is the total surface radiative energy. This is a major source for surface sensible and latent heat. The solar radiation (shortwave), Earth's longwave and transfer of atmospheric longwave makes the surface warmer (Shuttleworth, 2012). This also controls weather and climate extremes (Todd et al., 2000). The positive values suggest that the shortwave radiation is reflected back from the surface to the atmosphere (see Fig. S3). This makes the surface anomalously colder (see Figs. S3a–d). The negative value suggests anomalous increase of shortwave radiation at the surface; that is not transferred back to the atmosphere and trapped in the surface (Walden et al., 2017). This makes the surface anomalously warmer. Fig. S4 shows negative anomaly during all the events, suggesting anomalously increased longwave transfer to the atmosphere. It makes the surface colder and leads to the weather and climate variability. A strong negative anomaly shows comparatively colder and/or less warmer conditions (see Fig. S4d). Further, downwelling longwave and shortwave fluxes represent the energetics to determine the surface energy balance (Shuttleworth, 2012). The latent heat is employed for energy distribution and transfer from one place to another. Latent heat + Sensible heat = downward radiative energy + ground heat (Shuttleworth, 2012). A schematic representation is shown in Fig. S5, but not elaborated upon in the present work.

4. Conclusions

In the present study, the relationship between $\delta^{18}\text{O}$ proxy data of speleothem carbonates and model outputs over northeast and CMZ of India are used to enlarge understanding of the physical and dynamical processes/mechanisms of extremes during 850-2000AD viz., DC, MCA, EDC and LIA. Rationale for decreased precipitation and/or weakening of monsoon during these extremes is discussed based on palaeoclimate model fields.

During LIA, precipitation decreased over NEI relatively and increased over CMZ; whereas precipitation remained similar in present historical period (1850-2000AD) over NEI to that which prevailed during the LIA. However, during the EDC it was greater than the present scenario over NEI. The SPI shows decreased values during the EDC and increased values during the MCA. However, the maximum divergence is observed during the LIA suggesting frequent dry and wet spells. An inconsistent variation is observed in between near surface temperature

and cloud fraction. It suggests that the solar radiation was trapped during the cloudy condition resulting in the decrease of the surface temperature. However, the near surface temperature increased anomalously during the historical period (1850-2000AD). The increase in the near surface temperature may be possibly due to pre-industrial and post-industrial anthropogenic interventions (Zorita et al., 2005). The DTR shows significantly rising trend over the whole Indian subcontinent during the MCA and EDC. On the contrary, the LIA shows strong negative trend all over India except northern India. During the DC, abnormal transfer of latent heat from the surface is observed which makes the surface drier than normal (except in the Indo-Gangetic Plain). The anomaly in the sensible heat flux also indicates a significant pattern during the four extremes. It is observed that the sensible and latent heat is balanced by downward radiative flux (shortwave and longwave) but the remaining part is trapped inside the surface. Palaeoclimate models are subject to bias because of various limitations in simulations and parameter input; yet it is noteworthy that they are able to capture the signatures of extreme events in the past millennium.

This preliminary work highlights the importance of data-model intercomparison studies, in order to improve and enlarge our understanding of proxy-based palaeoclimate interpretations. However, there is need to still investigate, using palaeoclimate models, the heterogeneous regional distributions, model uncertainties, horizontal and vertical resolution during above extremes.

Code/data availability

Data is available under PMIP3 modeling experiment and grads software is used for preparing the figures. Secondary proxy data is collected from NCDC/NCEI.

Author contribution

APD conceived the idea and contributed while writing the manuscript; PK computed necessary data and contributed while writing the manuscript, SKT has provided guidance and improved the manuscript through critical comments.

Declaration of competing interest

The authors declare that they have no known competing financial interests or personal relationships that could have appeared to influence the work reported in this paper.

Acknowledgements

Authors acknowledge the National Climate Data Climate/National Centers for environmental information (NCDC/NCEI) and Earth System Grid Federation (ESGF-DKRZ) for permitting the free use of data from their data portals. PK thanks financial assistance from the University Grants Commission and Council of Scientific and Industrial Research, New Delhi, India.

Appendix A. Supplementary data

Supplementary data to this article can be found online at <https://doi.org/10.1016/j.quaint.2021.02.009>.

References

- Abram, N.J., Mulvaney, R., Vimeux, F., Phipps, S.J., Turner, J., England, M.H., 2014. Evolution of the southern annular mode during the past millennium. *Nat. Clim. Change* 4 (7), 564–569.
- Anderson, D.M., Overpeck, J.T., Gupta, A.K., 2002. Increase in the Asian southwest monsoon during the past four centuries. *Science* 297, 596–599. <https://doi.org/10.1038/nclimate2235>.

- Berkehammer, M., Sinha, A., Mudelsee, M., Cheng, H., Edwards, R.L., Cannariato, K., 2010. Persistent multidecadal power of the Indian summer monsoon. *Earth Planet Sci. Lett.* 290 (1–2), 166–172. <https://doi.org/10.1016/j.epsl.2009.12.017>.
- Berkehammer, M., Sinha, A., Stott, L., Cheng, H., Pausata, F.S., Yoshimura, K., 2012. An abrupt shift in the Indian monsoon 4000 years ago. *Clim. Landscapes Civil.* 75–88.
- Bowen, I.S., 1926. The ratio of heat losses by conduction and by evaporation from any water surface. *Phys. Rev.* 27 (6), 779. <https://doi.org/10.1103/PhysRev.27.779>.
- Bradley, R.S., Jones, P.D., 1992. When was the Little Ice Age. In: *Proceedings of the International Symposium on the Little Ice Age Climate*. Tokyo Metropolitan University, pp. 1–4.
- Bradley, R.S., Jones, P.D., 1993. 'Little Ice Age' summer temperature variations: their nature and relevance to recent global warming trends. *Holocene* 3 (4), 367–376.
- Briffa, K.R., 2000. Annual climate variability in the Holocene: interpreting the message of ancient trees. *Quat. Sci. Rev.* 19 (1–5), 87–105.
- Briffa, K.R., Jones, P.D., 1993. Global surface air temperature variations during the twentieth century: Part 2, implications for large-scale high-frequency palaeoclimatic studies. *Holocene* 3 (1), 77–88.
- Brown, J.R., Hope, P., Gergis, J., Henley, B.J., 2016. ENSO teleconnections with Australian rainfall in coupled model simulations of the last millennium. *Clim. Dynam.* 47 (1–2), 79–93. <https://doi.org/10.1007/s00382-015-2824-6>.
- Cayan, D.R., 1992. Latent and sensible heat flux anomalies over the northern oceans: driving the sea surface temperature. *J. Phys. Oceanogr.* 22 (8), 859–881. [https://doi.org/10.1175/1520-0485\(1992\)022<0859:LASHFA>2.0.CO;2](https://doi.org/10.1175/1520-0485(1992)022<0859:LASHFA>2.0.CO;2).
- Cook, E.R., Krusic, P.J., Jones, P.D., 2003. Dendroclimatic signals in long tree-ring chronologies from the Himalayas of Nepal. *Int. J. Climatol.: J. R. Meteorol. Soc.* 23 (7), 707–732.
- Crowley, T.J., Lowery, T.S., 2000. How warm was the medieval warm period? *AMBIO A J. Hum. Environ.* 29 (1), 51–55.
- D'Arrigo, R., Wilson, R., Li, J., 2006. Increased Eurasian-tropical temperature amplitude difference in recent centuries: implications for the Asian monsoon. *Geophys. Res. Lett.* 33 (22).
- Dimri, A.P., Kumar, D., Choudhary, A., Maharana, P., 2018. Future changes over the Himalayas: maximum and minimum temperature. *Global Planet. Change* 162, 212–234. <https://doi.org/10.1016/j.gloplacha.2018.01.015>.
- Dixit, Y., Tandon, S.K., 2016. Hydroclimatic variability of the Indian subcontinent in the past millennium: review and assessment. *Earth Sci. Rev.* 161, 1–15. <https://doi.org/10.1016/j.earscirev.2016.08.001>.
- Esper, J., Schweingruber, F.H., Winiger, M., 2002. 1300 years of climatic history for Western Central Asia inferred from tree-rings. *Holocene* 12 (3), 267–277.
- Gat, J.R., Gonfiantini, R., 1981. Stable Isotope Hydrology. Deuterium and Oxygen-18 in the Water Cycle. International Atomic Energy Agency, Vienna, ISBN 92-0-145281-0, 1981. STI/DOC/10/210.
- Grove, A., 1988. Two modellings for theory change. *J. Phil. Logic* 17 (2), 157–170.
- Gupta, A.K., Anderson, D.M., Overpeck, J.T., 2003. Abrupt changes in the Asian southwest monsoon during the holocene and their links to the North Atlantic ocean. *Nature* 421, 354–357. <https://doi.org/10.1038/nature01340>.
- Hegerl, G.C., Zwiers, F.W., Braconnot, P., Gillett, N.P., Luo, Y., Marengo Orsini, J.A., Nicholls, N., Penner, J.E., Stott, P.A., 2007. Understanding and attributing climate change. In: Solomon, S., Qin, D., Manning, M., Chen, Z., Marquis, M., Averyt, K.B., Tignor, M., Miller, H.L. (Eds.), *Climate Change 2007: The Physical Science Basis. Contribution of Working Group I to the Fourth Assessment Report of the Intergovernmental Panel on Climate Change*. Cambridge University Press, Cambridge, United Kingdom and New York, NY, USA.
- Hessl, A.E., Anchukaitis, K.J., Jelsema, C., Cook, B., Byambasuren, O., Leland, C., Nachin, B., Pederson, N., Tian, H., Hayles, L.A., 2018. Past and future drought in Mongolia. *Sci. Adv.* 4 (3), e1701832 <https://doi.org/10.1126/sciadv.1701832>.
- Hughes, M.K., Diaz, H.F. (Eds.), 1994a. *The Medieval Warm Period*, vol. 22. Springer Science & Business Media.
- Hughes, M.K., Diaz, H.F., 1994b. Was there a 'medieval warm period', and if so, where and when? *Climatic Change* 26 (2–3), 109–142.
- Jones, P.D., Mann, M.E., 2004. Climate over past millennia. *Rev. Geophys.* 42 (2).
- Jones, P.D., Briffa, K.R., Barnett, T.P., Tett, S.F.B., 1998. High-resolution palaeoclimatic records for the last millennium: interpretation, integration and comparison with General Circulation Model control-run temperatures. *Holocene* 8 (4), 455–471.
- Jukes, M.N., Allen, M.R., Briffa, K.R., Esper, J., Hegerl, G.C., Moberg, A., Osborn, T.J., Weber, S.L., 2007. Millennial temperature reconstruction intercomparison and evaluation. *Clim. Past* 3 (4), 591–609.
- Kathayat, G., Cheng, H., Sinha, A., Spötl, C., Edwards, R.L., Zhang, H., Li, X., Yi, L., Ning, Y., Cai, Y., Lui, W.L., 2016. Indian monsoon variability on millennial-orbital timescales. *Sci. Rep.* 6, 24374. <https://doi.org/10.1038/srep24374>.
- Kotlia, B.S., Ahmad, S.M., Zhao, J.X., Raza, W., Collerson, K.D., Joshi, L.M., Sanwal, J., 2012. Climatic fluctuations during the LIA and post-LIA in the Kumaon Lesser Himalaya, India: evidence from a 400 y old stalagmite record. *Quat. Int.* 263, 129–138.
- Kumar, P., Sanwal, J., Dimri, A.P., Ramesh, R., 2019. Contribution of diverse monsoon precipitation over central and northern India during mid to late holocene. *Quat. Int.* 507 <https://doi.org/10.1016/j.quaint.2018.10.003>.
- Le, T., 2015. Solar forcing of Earth's surface temperature in PMIP3 simulations of the last millennium. *Atmos. Sci. Lett.* 16 (3), 285–290.
- Lechleitner, F.A., Breitenbach, S.F., Cheng, H., Plessen, B., Rehfeld, K., Goswami, B., Marwan, N., Eroglu, D., Adkins, J., Haug, G., 2017. Climatic and in-cave influences on $\delta^{18}O$ and $\delta^{13}C$ in a stalagmite from northeastern India through the last deglaciation. *Quat. Res.* 88 (3), 458–471.
- Li, X., Zhang, R., Zhang, Z., Yan, Q., 2018. Do climate simulations support the existence of East Asian monsoon climate in the Late Eocene? *Palaeogeogr. Palaeoclimatol. Palaeoecol.* <https://doi.org/10.1016/j.palaeo.2017.12.037>.
- Liu, Jian, Wang, Bin, Cane, Mark A., Yim, So-Young, Lee, June-Yi, 2013. Divergent global precipitation changes induced by natural versus anthropogenic forcing. *Nature* 493 (7434), 656.
- Ljungqvist, F.C., 2010. A new reconstruction of temperature variability in the extra-tropical Northern Hemisphere during the last two millennia. *Geogr. Ann. Phys. Geogr.* 92 (3), 339–351.
- Loehle, C., 2007. A 2000-year global temperature reconstruction based on non-treering proxies. *Energy Environ.* 18 (7), 1049–1058.
- Lu, E., Luo, Y., Zhang, R., Wu, Q., Liu, L., 2011. Regional atmospheric anomalies responsible for the 2009–2010 severe drought in China. *J. Geophys. Res.: Atmosphere* 116 (D21).
- Mann, M.E., Jones, P.D., 2003. Global surface temperatures over the past two millennia. *Geophys. Res. Lett.* 30 (15).
- Mann, M.E., Bradley, R.S., Hughes, M.K., 1999. Northern hemisphere temperatures during the past millennium: inferences, uncertainties, and limitations. *Geophys. Res. Lett.* 26 (6), 759–762.
- Mann, M.E., Zhang, Z., Hughes, M.K., Bradley, R.S., Miller, S.K., Rutherford, S., Ni, F., 2008. Proxy-based reconstructions of hemispheric and global surface temperature variations over the past two millennia. *Proc. Natl. Acad. Sci. U.S.A.* 105 (36), 13252–13257.
- Mann, M.E., Zhang, Z., Rutherford, S., Bradley, R.S., Hughes, M.K., Shindell, D., Ammann, C., Faluvegi, G., Ni, F., 2009. Global signatures and dynamical origins of the little ice age and medieval climate anomaly. *Science* 326 (5957), 1256–1260.
- McGregor, H.V., Evans, M.N., Goosse, H., Leduc, G., Martrat, B., Addison, J.A., Phipps, S. J., 2015. Robust global ocean cooling trend for the pre-industrial Common Era. *Nat. Geosci.* 8 (9), 671–677.
- Moberg, A., Sonechkin, D.M., Holmgren, K., Datsenko, N.M., Karlén, W., 2005. Highly variable Northern Hemisphere temperatures reconstructed from low-and high-resolution proxy data. *Nature* 433 (7026), 613.
- Nagarajan, R., 2010. *Drought Assessment*. Springer Science & Business Media.
- Ning, L., Liu, J., Wang, Z., Bradley, R.S., 2018. Different influences on the tropical Pacific SST gradient from natural and anthropogenic forcing. *Int. J. Climatol.* 38 (4), 2015–2028.
- Oke, T.R., 1982. The energetic basis of the urban heat island. *Q. J. R. Meteorol. Soc.* 108 (455), 1–24.
- Osborn, T.J., Briffa, K.R., 2006. The spatial extent of 20th-century warmth in the context of the past 1200 years. *Science* 311 (5762), 841–844.
- Phipps, S.J., Rotstayn, L.D., Gordon, H.B., Roberts, J.L., Hirst, A.C., Budd, W.F., 2012. The CSIRO Mk3L climate system model version 1.0-Part 2: response to external forcings. *Geosci. Model Dev. (GMD)* 5 (3), 649.
- Rai, P., Joshi, M., Dimri, A.P., Turner, A.G., 2019. The role of potential vorticity anomalies in the Somali jet on Indian summer monsoon intraseasonal variability. *Clim. Dynam.* 50 (11–12), 4149–4169.
- Rühland, K., Phadtare, N.R., Pant, R.K., Sangode, S.J., Smol, J.P., 2006. Accelerated melting of Himalayan snow and ice triggers pronounced changes in a valley peatland from northern India. *Geophys. Res. Lett.* 33 <https://doi.org/10.1029/2006GL026704>.
- Sanwal, J., Kotlia, B.S., Rajendran, C., Ahmad, S.M., Rajendran, K., Sandiford, M., 2013. Climatic variability in Central Indian Himalaya during the last–1800 years: evidence from a high resolution speleothem record. *Quat. Int.* 304, 183–192.
- Sellers, W.D., 1965. *Physical Climatology* (No. 551.6 S467). University of Chicago Press, p. 272. <https://doi.org/10.1177/0309133308096757>.
- Shi, G., Ribbe, J., Cai, W., Cowan, T., 2008. An interpretation of Australian rainfall projections. *Geophys. Res. Lett.* 35 (2) <https://doi.org/10.1029/2007GL032436>.
- Shuttleworth, W.J., 2012. Surface energy fluxes. *Terrestrial Hydrometeorol.* <https://doi.org/10.1002/9781119951933>.
- Sinha, A., Cannariato, K.G., Stott, L.D., Cheng, H., Edwards, R.L., Yadava, M.G., Ramesh, R., Singh, I.B., 2007. A 900-year (600 to 1500 AD) record of the Indian summer monsoon precipitation from the core monsoon zone of India. *Geophys. Res. Lett.* 34, L16707. <https://doi.org/10.1029/2007GL030431>.
- Sinha, A., Berkehammer, M., Stott, L., Mudelsee, M., Cheng, H., Biswas, J., 2011. The leading mode of Indian Summer Monsoon precipitation variability during the last millennium. *Geophys. Res. Lett.* 38 (15) <https://doi.org/10.1029/2011GL047713>.
- Spittlehouse, D.L., Black, T.A., 1980. Evaluation of the Bowen ratio/energy balance method for determining forest evapotranspiration. *Atmos.-Ocean* 18 (2), 98–116.
- Su, Z., 2002. The Surface Energy Balance System (SEBS) for estimation of turbulent heat fluxes. *Hydrol. Earth Syst. Sci.* 6 (1), 85–100.
- Sun, X.B., Ren, G.Y., Shrestha, A.B., Ren, Y.Y., You, Q.L., Zhan, Y.J., Rajbhandari, R., 2017. Changes in extreme temperature events over the hindu kush Himalaya during 1961–2015. *Adv. Clim. Change Res.* 8 (3), 157–165.
- Tejavath, C.T., Karumuri, A., Chakraborty, S., Ramesh, R., 2017. The Indian summer monsoon climate during the Last Millennium, as simulated by the PMIP3. *Clim. Past Discuss.* <https://doi.org/10.5194/cp-2017-24> [preprint], 2017.
- Tejavath, C.T., Ashok, K., Chakraborty, S., Ramesh, R., 2018. The ENSO teleconnections to the Indian summer monsoon climate through the Last Millennium as simulated by the PMIP3. *Clim. Past Discuss.* <https://doi.org/10.5194/cp-2018-7>.
- Tiwari, M., Ramesh, R., Yadava, M.G., Somayajulu, B.L.K., Jull, A.J.T., Burr, G.S., 2006. Is there a persistent control of monsoon winds by precipitation during the late Holocene? *Geochem. Geophys. Geosyst.* 7, Q03001. <https://doi.org/10.1029/2005GC001095>.
- Todd, R.W., Evett, S.R., Howell, T.A., 2000. The Bowen ratio-energy balance method for estimating latent heat flux of irrigated alfalfa evaluated in a semi-arid, advective environment. *Agric. For. Meteorol.* 103 (4), 335–348.
- Veena, M.P., Achyuthan, H., Eastoe, C., Farooqui, A., 2014. A multi-proxy reconstruction of monsoon variability in the late Holocene, South India. *Quat. Int.* 325, 63–73.

- Walden, V.P., Hudson, S.R., Cohen, L., Murphy, S.Y., Granskog, M.A., 2017. Atmospheric components of the surface energy budget over young sea ice: results from the N-ICE2015 campaign. *J. Geophys. Res.: Atmosphere* 122 (16), 8427–8446.
- Wang, B., Xiang, B., Li, J., Webster, P.J., Rajeevan, M.N., Liu, J., Ha, K.J., 2015. Rethinking Indian monsoon rainfall prediction in the context of recent global warming. *Nat. Commun.* 6, 7154.
- Yadava, M.G., Ramesh, R., 2005. Monsoon reconstruction from radiocarbon dated tropical Indian speleothems. *Holocene* 15 (1), 48–59.
- Yadava Madhusudan, G., 2002. Stable Isotope Systematics in Cave Calcites: Implications to Past Climatic Changes in Tropical India. Physical Research Laboratory, Ahmedabad, India (Ph. D. thesis).
- Yaocun, Z., Dongqian, W., Xuejuan, R., 2008. Seasonal variation of the meridional wind in the temperate jet stream and its relationship to the Asian monsoon. *Acta Meteorol. Sin.* 22, 446–454.
- Zorita, E., González-Rouco, J.F., Von Storch, H., Montávez, J.P., Valero, F., 2005. Natural and anthropogenic modes of surface temperature variations in the last thousand years. *Geophys. Res. Lett.* 32 (8) <https://doi.org/10.1029/2004GL021563>.